Annals of Biomedical Engineering, Vol. 29, pp. 854–861, 2001
Printed in the USA.

0090-6964/2001/29(10)/854/8/$15.00

Phase Shifting Prior to Spatial Filtering Enhances Optical Recordings of Cardiac Action Potential Propagation

DERRICK SUNG,[1,3] JYOTSNA SOMAYAJULA-JAGAI,[2] PAMELA COSMAN,[2] ROBERT MILLS,[1,3] and ANDREW D. MCCULLOCH[1,3]

[1]Department of Bioengineering, University of California San Diego, La Jolla, CA, [2]Department of Electrical and Computer Engineering, University of California San Diego, La Jolla, CA, and [3]The Whitaker Institute of Biomedical Engineering, University of California San Diego, La Jolla, CA

(Received 6 July 2001; accepted 7 July 2001)

Abstract—Optical imaging of cardiac electrical activity using a voltage-sensitive dye provides high spatial resolution maps of action potential propagation and repolarization. Charge-coupled-device (CCD) camera-based imaging systems, however, are limited by their low signal-to-noise ratio. We have developed an image processing method to enhance the quality of optical signals recorded using a CCD camera. The method is based on the observation that within a small neighborhood of adjacent pixels, the morphology of the optical action potential varies little except for a phase shift in time resulting from the propagation of the wavefront. The method uses a phase-correlation technique to first correct for this time shift before spatially filtering with a 5×5 Gaussian convolution kernel ($\sigma=1.179$). A length 5 median filter is then applied to further reduce noise by filtering in the temporal domain. The image-processing scheme allows for more accurate extraction of maps of electrical activation, repolarization, and action potential duration. © *2001 Biomedical Engineering Society.*
[DOI: 10.1114/1.1408927]

Keywords—Voltage-sensitive dye, Optical mapping, Image processing, Electrophysiology.

INTRODUCTION

Optical recording of electrical activity in the heart using a voltage-sensitive dye has proven to be a useful tool in investigating patterns of cardiac action potential propagation and repolarization. Unlike intracellular and extracellular electrode recording techniques, optical recordings do not require physical contact with the myocardium and can thus provide high resolution spatial maps of electrical activity. Cardiac optical mapping has been used in a variety of preparations ranging from the single cell[17,19] to the intact organ.[4,6,10] Applications have included imaging the patterns of ventricular fibrillation,[8,20] reentrant phenomena,[7,14] and the conduction pathway through the atrioventricular node.[3]

Address correspondence to Andrew D. McCulloch, PhD, UCSD, Department of Bioengineering, 9500 Gilman Dr., La Jolla, CA 92093-0412. Electronic mail: amcculloch@ucsd.edu

The basis of the optical recording is the voltage sensitive fluorescent dye whose fluorescence intensity varies in response to transmembrane potential.[12] The dyes have a very fast response time on the order of microseconds. Thus, the temporal resolution achievable by optical mapping is currently limited by the recording technology rather than by the response of the dye. The two primary hardware configurations used for recording optical signals involve either photodiode arrays or charge-coupled-device (CCD) cameras. Photodiode arrays can provide high sensitivity with good quantum efficiency and low dark current, and high temporal resolutions in excess of 1 kHz, but their spatial resolution is limited to less than 500 or so total elements (commercially available arrays greater than 256 elements are difficult to find). CCD cameras, on the other hand, can provide over 100 times the spatial resolution of photodiode arrays and are available off the shelf; however CCD camera systems are limited by their poor signal-to-noise ratio and relatively lower temporal resolution.

Since CCD camera-based optical imaging is more severely limited in temporal than spatial resolution, we have developed a new combination of temporal and spatial filtering techniques to enhance the information content of activation and repolarization maps. The approach makes use of two basic properties of the spread of electrical excitation throughout the myocardium: (1) impulses propagate in a wave-like fashion across the heart surface; and (2) in general the morphology of the optical action potential normally does not vary greatly within a small neighborhood of adjacent pixels. These observations allow the spatial filtering to be improved by first adjusting for phase shifts between neighboring signals.

IMAGE ACQUISITION

Experimental Methods

All data were acquired from the epicardium of isolated Langendorff perfused rabbit hearts. The experimental preparation used has been previously described.[18]

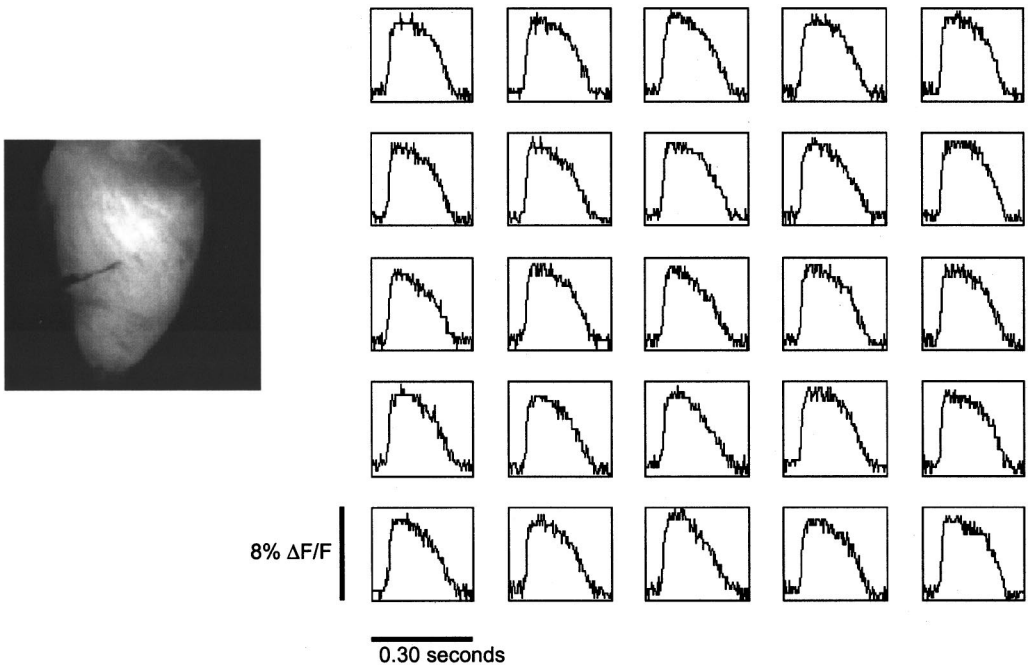

FIGURE 1. Normalized raw optical action potentials extracted from a 5×5 pixel region of the image shown on the left. Each tracing represents the local electrical activity at a distinct image pixel.

Briefly, the heart of an anesthetized New Zealand white rabbit was exposed, arrested, and rapidly excised. The coronary arteries were perfused with a warm (35–37°C) oxygenated (95% O_2, 5% CO_2) modified Tyrodes solution. The electromechanical decoupling agent 2,3 butanedione monoxime (15 mM) was added to the perfusate to reduce motion artifact. The tissue was stained with a 10 ml bolus injection of the voltage sensitive dye, di-4-ANEPPS (10.4 μM), into the coronary arteries. The heart was paced at 240 beats per minute from the left ventricular epicardium using a bipolar electrode at approximately twice diastolic threshold.

Hardware Configuration

The hardware setup has also been described in a previous publication.[18] Excitation light from a 300 W Xe arc lamp (Oriel Instruments, Stratford, CT) was passed through a dichroic mirror to filter out UV and IR components and subsequently through a 516 ± 45 nm bandpass filter. The excitation light beam was then split with a bifurcating fiber optic bundle and directed as uniformly as possible onto the surface of the left ventricular free wall. An electronic shutter limited the exposure of the heart to the excitation light to a few seconds per run, thus minimizing the phototoxic and photobleaching effects of the dye.

The emitted fluorescence from the heart was passed through a >610 nm high pass filter and focused with a fast 50 mm lens (1:0.95, Navitar, Rochester, NY) onto an 8-bit CCD camera (Dalsa, Waterloo, Ontario model CA-D1-256). The camera had a base pixel resolution of 256×256 but was operated in a binning mode in which the charge from adjacent pixels was combined, increasing sensor sensitivity while reducing resolution. The result was a final spatial resolution of 128×128 at a rate of 399 frames per second.

IMAGE PROCESSING

All image processing algorithms were developed using the MATLAB programming environment. The image processing routines were run on a Silicon Graphics Octane workstation with a 350 MHz MIPS R12000 processor.

Preprocessing

An optical signal was obtained from each pixel on the surface of the heart in the time series of fluorescent images (Fig. 1). Depolarization of the myocardial tissue results in a decrease in dye fluorescence intensity, so the signals were first inverted to better represent a cellular action potential. The background diastolic 8-bit intensity value was calculated by taking the median value of all points within the lowest 20% of the signal range. The signals were then normalized by calculating the fractional change in fluorescence compared to the background diastolic signal ($\Delta F/F$). Plots of the normalized raw optical action potentials are shown in Figs. 1 and 2(b).

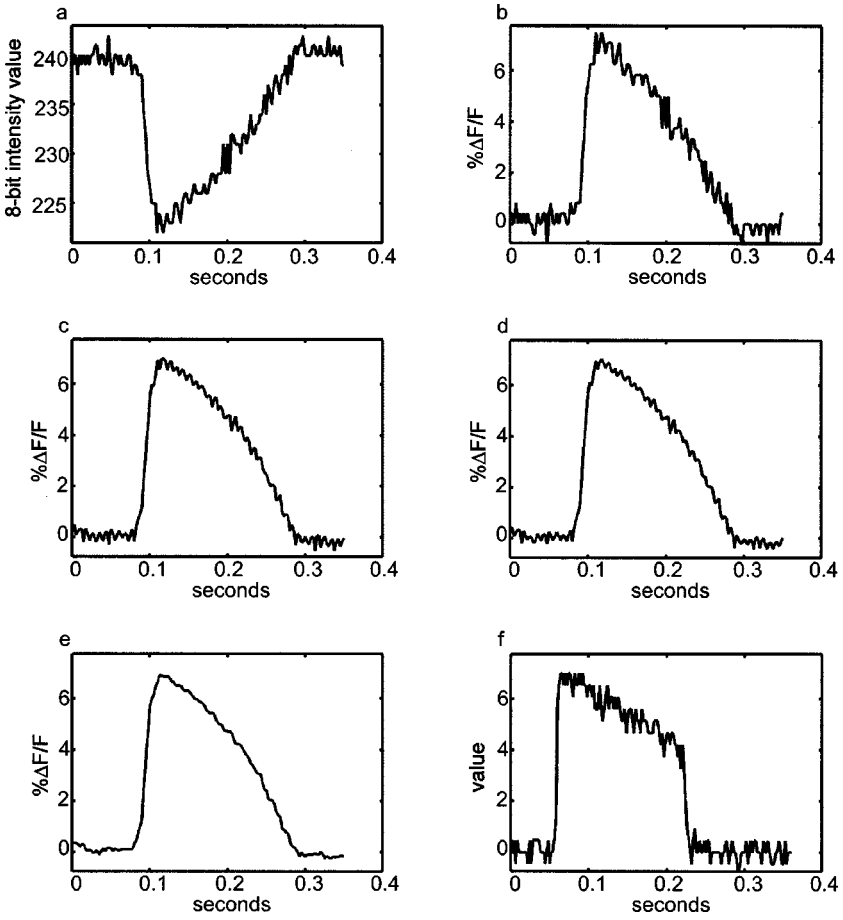

FIGURE 2. (a) Representative raw optical action potential from a single pixel location; (b) the signal after inversion and normalization; (c) the signal following 5×5 spatial filtering without phase shifting; (d) the signal following 5×5 spatial filtering with phase shifting; (e) the final signal after length 5 median temporal filtering; (f) a representative model signal before filtering.

Phase-Shift Spatial Filtering

Given that the morphology of the raw signals within a local neighborhood of pixels varies quite modestly (Fig. 1), it was concluded that spatial averaging would provide an effective means of noise reduction. However, the situation was complicated by the fact that the signal was not only varying in time, but was also moving as a wavefront, varying in space. Epicardial conduction velocities in the rabbit heart range between 15 and 80 cm/s.[15,18] At the pixel resolution and magnification of our system, this translates to a temporal shift in the signal of 2–0.4 ms, respectively, between adjacent pixels. Failing to correct for this shift would result in a blurring of the signal and loss of key features such as the sharp upstroke of depolarization.

Therefore, a phase-correlation technique was employed to correct for this time shift prior to performing any spatial filtering. The phase-correlation method is often used to compute the shift in time signals collected by a sensor array.[9] The principle behind the technique is as follows:

Let f_2 be the time-shifted version of f_1:

$$f_2(t)=f_1(t-t_0).$$

Taking the Fourier transform of both sides gives

$$F_2(u)=e^{-j2\pi ut_0}F_1(u),$$

and therefore

$$\frac{F_2(u)F_1^*(u)}{|F_1(u)F_1^*(u)|}=e^{-j2\pi ut_0}.$$

Taking the inverse transform gives an impulse function which is centered at the shift, t_0.

The measured optical action potential was not exactly a time-shifted version of its neighbor, but also differed as a result of noise and as a result of any underlying morphological changes. In general, the latter differences were negligible within a neighborhood of adjacent pixels. The noise differences between adjacent pixels could be substantial, but the phase-correlation method has been shown to be very robust against noise.[2,11] In the presence of noise, the inverse transform of the ratio yielded an approximate discrete delta function, but the peak of the function could still be used reliably to ascertain the shift.

The signals were spatially filtered using a centered 5×5 Gaussian convolution kernel ($\sigma=1.179$). Thus, for each pixel, the relative phase shifts of the surrounding 24 signals were calculated using the above method. Before calculating phase shifts, all action potentials were interpolated in time by a factor of 10 so that subframe phase shifts could be resolved. The interpolation algorithm employed a low-pass finite impulse response (FIR) filter, which allowed the original data to pass through unchanged and interpolated between so that the mean-square errors between the interpolated points and their ideal values were minimized. The signals from the surrounding pixels were shifted to be in phase with the center pixel, and then were decimated without low-pass filtering back to original temporal resolution. After phase shifting, the convolution kernel was applied to the neighborhood for each frame. Figures 2(c) and 2(d) show the signal after spatial filtering without and with phase shifting.

Temporal Filtering

After the signals were spatially filtered, the signal quality was further enhanced by the application of a temporal filter. The three types of temporal filters considered were centered median filters of lengths 3,5,7, and 9, a low-pass Kaiser window filter ($\beta=5.5,\omega_p=0.2,\omega_s=0.6,\delta=0.001$), and a mean-value filter of length 5. The median filter of length 5 was chosen because it best preserved the steep upstroke of the optical action potential, a key feature in determining the activation time. A representative plot of the final filtered signal is shown in Fig. 2(e).

Feature Extraction

Once the images were filtered, we were able to apply an algorithm to extract and map key features from the optical action potentials. The activation times were identified as the time of maximum first derivative of the action potential upstroke. Prior to calculating activation time, the signals were again interpolated by a factor of 10 to attain subframe resolution of activation time. Figure 3 shows the activation, repolarization, and action potential duration (APD) maps recorded during an episode of left ventricular epicardial pacing. Figure 3(a) shows activation maps generated from the unfiltered raw signals, unshifted but filtered signals, and phase-shifted then filtered signals using the same activation time algorithm. Note how the unshifted map appears blurred compared with the phase-shifted maps.

To calculate action potential repolarization time, the peak of the signal following the upstroke was first identified. Action potential repolarization time was computed by determining the time at which the optical action potential had recovered 80% from the peak value. Figure 3(b) maps the 80% repolarization times calculated from the unfiltered images and after the application of the two different filtering schemes. The pattern of repolarization is also much crisper in the phase-shifted images. The APD maps in Fig. 3(c) were calculated by subtracting the activation time from the 80% repolarization time-ateach pixel. The filtering process is particularly important when extracting APD maps, as the slight errors in activation and repolarization times incurred without phase shifting are amplified in the APD map [Fig. 3(c)], and may cause artifactual alterations in any estimation of the dispersion of APD. The dispersion of action potential duration is often used as an index of arrythmogenicity.

VALIDATION

To quantify the effects of the signal processing scheme on signal accuracy, a propagating action potential was simulated using a modified FitzHugh–Nagumo model.[16] A 16×32 finite element mesh was constructed representing a 5×10 mm rectangle of tissue, which is comparable to that recorded in our experiments. The model was sampled at 500 Hz at the nodes, giving a spatial and temporal resolution comparable to those used in experiments. The diffusion coefficients were set to give an approximate conduction velocity of 20 cm/s in the cross-fiber direction and 30 cm/s in the fiber direction, which are within the ranges observed in experiments. This combination of parameters resulted in a phase shift between nodes of 1.0–1.5 ms, thus, the range of phase shifts within a pixel neighborhood was the same as or greater than the sampling period of 2 ms. The signals were scaled to cover a range of 15, which is similar to the range of the measured 8-bit intensity valued optical action potentials. Gaussian noise ($\sigma=0.7$) was independently added to each signal, after which the signals were rounded to the nearest integer, resulting in quantized noisy signals like those observed in experiments. The signals were then rescaled to a range of 6, corresponding to the range of experimental signals after normalization [Fig. 2(f)]. The data set was then filtered using the above algorithm.

Four error measures were used to evaluate signal quality. These error measures were all percent differences between the final filtered signal and the original simulated signal (before noise had been added), specifically: (1) percent mean signed difference of the rate of depolarization, calculated by sequence averaging the difference of the rate of depolarization throughout the upstroke for each signal, and dividing by the ensemble average of the maximum rate of depolarization; (2) percent mean absolute difference of the signal magnitude during repolarization, calculated by sequence averaging the absolute difference of the signal throughout repolarization (signal peak to 80% recovery), then dividing by

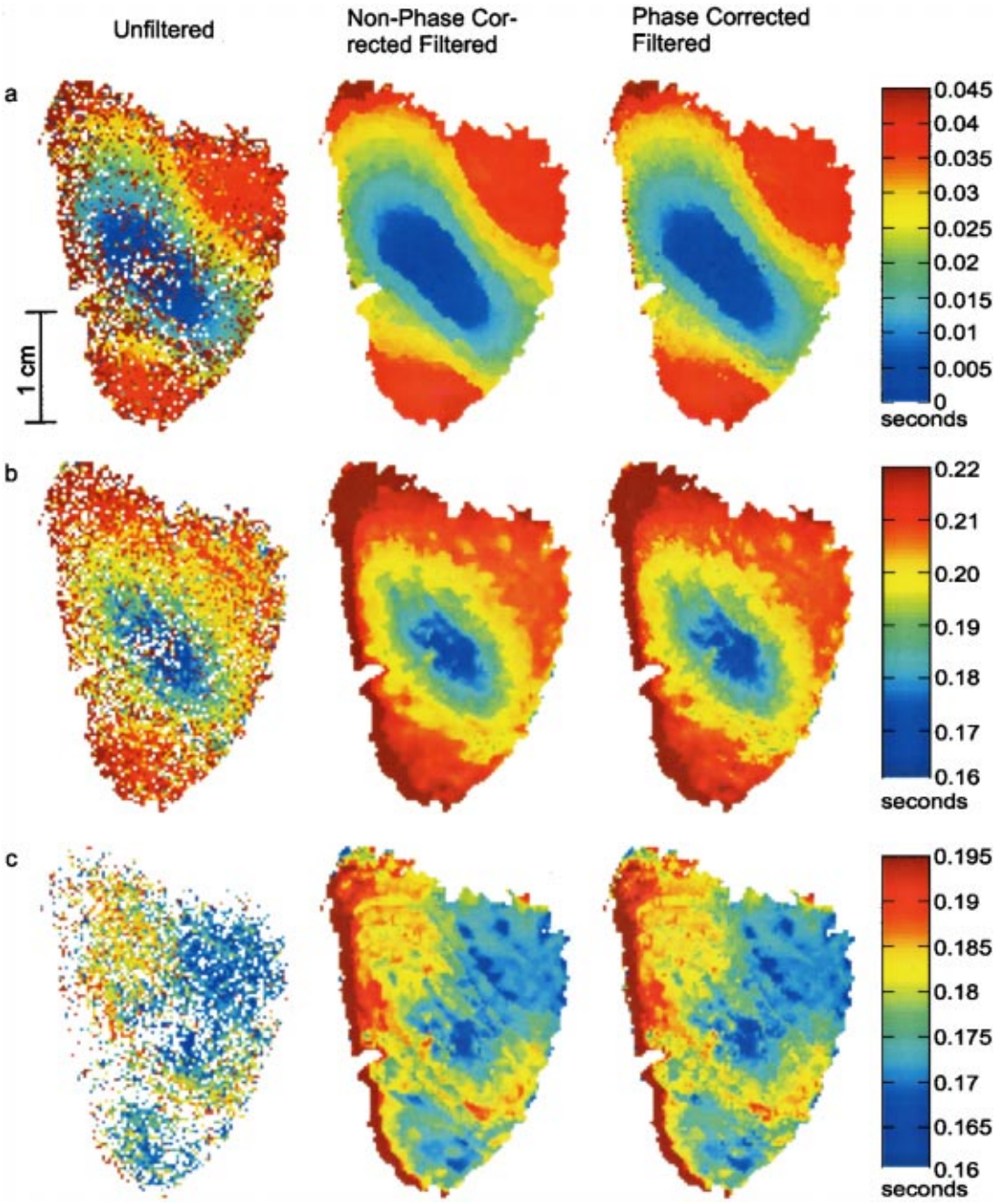

FIGURE 3. (a) Activation maps, (b) repolarization maps, and (c) action potential duration maps extracted from unfiltered, unshifted but filtered, and phase-shifted then filtered images.

the ensemble average of the maximum signal magnitude (during repolarization); (3) and (4) percent signed difference of activation and repolarization times (as determined by the feature extraction algorithm described above), calculated by taking the signed difference for each signal, and dividing by the ensemble average of action potential duration (as defined above).

Table 1 shows the distribution statistics of the above error measures calculated from the application of three different Gaussian convolution kernels: 3×3 ($\sigma=0.631$), 5×5 ($\sigma=1.179$), and 7×7 ($\sigma=1.475$) with and without phase shifting. The actual coefficients of the filters are listed in the Appendix. Without the phase shifting, the 3×3 filter resulted in a modest improvement in signal quality, as seen in the decrease of depolarization rate error deviation, repolarization error, and repolarization error deviation. Application of the larger sized filters decreased repolarization error and deviation, but worsened depolarization rate error and deviation due to the blurring effects discussed previously. Incorporating the

TABLE 1. Error distribution statistics of AP characteristics.[a]

	Unfiltered	3×3 $\sigma=0.631$	5×5 $\sigma=1.179$	7×7 $\sigma=1.475$
	Percent mean signed difference of the rate of depolarization			
Unshifted	0.06±3.80	5.85±2.30	12.88±3.93	18.43±4.88
Phase-shifted		1.55±1.70	0.78±1.11	0.63±0.98
	Percent mean absolute difference of the signal magnitude during repolarization			
Unshifted	4.00±0.53	1.11±0.23	0.65±0.15	0.57±0.14
Phase-shifted		1.06±0.23	0.61±0.13	0.49±0.11
	Percent signed difference of activation time			
Unshifted	0±2.00	0±0.20	0±0.35	0±0.47
Phase-shifted		0±0.13	0±0.11	0±0.11
	Percent signed difference of repolarization time			
Unshifted	0±0.36	−0.12±0.19	−0.24±0.27	−0.36±0.36
Phase-shifted		0±0.19	0±0.13	0±0.12

[a]Values were computed following the application of three different sized Gaussian convolution kernels (3×3, 5×5, 7×7) without and with phase shifting.

phase shifting improved signal quality compared to the unshifted for all three kernel sizes. The phase shifting significantly decreased the depolarization rate error and deviation. The decrease in signed error indicates that the algorithm attenuates a systematic error that reduces measured upstroke rate when filtering without phase shifting. The effect on signal-to-noise ratio due to phase shifting was not appreciable. Phase shifting also removes a systematic error in the calculation of repolarization time. Though the best signal quality was achieved with the 7×7 filter, the additional improvement was only slightly better than that achieved with the 5×5 kernel, and comes at a significantly greater computational cost.

We independently evaluated the effectiveness of the filtering process using experimentally derived information. Thirty raw optical action potentials were randomly sampled from four different hearts. For each signal, an ideal was carefully generated by hand according to the following criteria: The resting baseline signal was taken as the mean signal before the start of the upstroke, which was determined by eye. The slope of the upstroke was drawn to match the slope of the raw signal, and the peak was calculated from an average of peak values in the raw signal. The shape of the plateau and repolarization were traced out by hand, and the end-systolic baseline value was calculated by averaging the last 10 points from the raw signal. The mean-squared errors between the ideal and the filtered signals (both with and without phase shifting) were calculated to measure the effectiveness of the filtering process. The conclusions drawn from these validation procedures were consistent with those reached using model-simulated test data.

DISCUSSION

CCD camera-based optical mapping provides a powerful noncontact tool to visualize electrical activity in the heart. The advantage of a CCD camera-based system lies in its ability to capture data at very high spatial resolutions, but the method can be limited by the large amounts of noise in the recorded signals. This limitation can be thought of as a tradeoff between signal quality and spatial resolution. We have developed an image processing technique to overcome this limitation by taking advantage of the dense spatial information to enhance the quality of the signal through filtering. Our technique is based on the observation that the morphology of the optical action potentials within a local neighborhood varies only by a phase shift in time.

Other investigators using camera-based optical mapping systems have incorporated spatial filtering methods without considering the phase characteristics of the signal.[1,20] By correcting for this phase shift, we were able to filter over a much larger local area without loss of signal accuracy and with much better results (Table 1). The wave-based properties of electrical activation have been used before to interpolate activation time data from sparse arrays of electrocardiogram leads,[13] but the method presented here represents the first time that such information has been incorporated into a noise reduction filtering process for optically recorded signals.

A limitation to our technique is the assumption that the morphology of the optical action potentials remains constant within the local area of averaged pixels. This assumption may be affected by the local properties of the

myocardium or by the phenomena being imaged. For example, the morphology of the action potential changes near the rotor of a reentrant scroll wave. External factors such as the nonuniformity of the light source and the magnification of the image would also affect local homogeneity of the recorded optical action potentials. For situations where there is a high degree of local heterogeneity in the signals, we would need to decrease the area over which the signals are averaged. This could be achieved by reducing the pixel area of the sliding filter or by increasing the magnification of the image.

The phase-shift image processing routine requires that the heart be free from motion during the optical recordings. This was achieved in our preparation using the pharmacological agent 2,3 butanedione monoxime. Other investigators have eliminated motion blur during optical recordings by mechanically stabilizing the heart.[4,5] With the motion eliminated, each image pixel reflects the local electrical activity at a fixed location on the epicardium.

Furthermore, the improvement in signal quality due to phase shifting was not substantial until the range of phase shifts within the pixel neighborhood used for spatial averaging was equal to or greater than the sampling period. The range of phase shifts is influenced by many factors. As spatial resolution or conduction velocity increases, the range of neighborhood phase shifts decreases. However, camera capabilities and the area of tissue that is imaged limit spatial resolution. Increasing temporal resolution or the size of the spatial filter will increase the range of phase shifts. Thus, as optical mapping studies are performed in mice, for example, the increase in conduction velocity and spatial resolution will be offset by the required increase in sampling frequency to resolve the action potentials properly, bolstering the utility of this algorithm.

Another limitation is the significant increase in computational overhead required by the phase-shifting algorithm. It took 53 min of computational time using the phase-shift filtering routine to process 6049 signals, 141 points in length, with a 5×5 kernel, compared to 26 min to perform the spatial filtering without the phase shifting. However, our algorithm was developed using interpretive MATLAB code that was not optimized. However, simple morphology checks can be used to determine which pixels of the frame are not within the region of interest and therefore can be excluded from further calculations.

The image processing method presented will further expand the capabilities of a CCD camera-based optical mapping system. It can be directly incorporated into a model-based parametric analysis of conduction velocity.[18] The filtering technique allows for more precise determination of activation and repolarization times while retaining high spatial resolution. Such a data processing technique, coupled with the ever improving hardware technologies that are becoming available, will allow for more detailed visualizations of the complex spatiotemporal electrical phenomena which make up ventricular fibrillation and other clinically relevant arrhythmias.

APPENDIX

The following three Gaussian convolution kernels were used to generate the values in Table 1.

	Standard deviation (σ)	Coefficients
3×3 kernel	0.631	$\frac{1}{32}\begin{bmatrix}1&4&1\\4&12&4\\1&4&1\end{bmatrix}$
5×5 kernel	1.179	$\frac{1}{146}\begin{bmatrix}1&3&4&3&1\\3&9&12&9&3\\4&12&18&12&4\\3&9&12&9&3\\1&3&4&3&1\end{bmatrix}$
7×7 kernel	1.475	$\frac{1}{264}\begin{bmatrix}0&1&2&3&2&1&0\\1&3&6&8&6&3&1\\2&6&13&16&13&6&2\\3&8&16&20&16&8&3\\2&6&13&16&13&6&2\\1&3&6&8&6&3&1\\0&1&2&3&2&1&0\end{bmatrix}$

ACKNOWLEDGMENTS

The authors gratefully acknowledge the assistance of Taras Usyk for the model data, and Babak Fazeli and Zhuangjie Li during the experimental procedures. This research was supported in part by NSF Grant Nos. BES-9634974, BES-0086482, MIP-9624729, and the National Biomedical Computation Resource, NIH P41 Grant No. RR08605. One of the authors (D.S.) was supported by NIH training Grant No. T32HL07444.

REFERENCES

[1] Baxter, W. T., J. M. Davidenko, L. M. Loew, J. P. Wuskell, and J. Jalife. Technical features of a CCD video camera system to record cardiac fluorescence data. *Ann. Biomed. Eng.* 25:713–725, 1997.

[2] De Castro, E., and C. Morandi. Registration of translated and rotated images using finite Fourier transforms. *IEEE Trans. Pattern Anal. Mach. Intell.* PAMI-9:700–703, 1987.

[3] Efimov, I. R., G. J. Fahy, Y. Cheng, D. R. Van Wagoner, P. J. Tchou, and T. N. Mazgalev. High-resolution fluorescent imaging does not reveal a distinct atrioventricular nodal anterior input channel (fast pathway) in the rabbit heart during sinus rhythm. *J. Cardiovasc. Electrophys.* 8:295–306, 1997.

[4] Efimov, I. R., D. T. Huang, J. M. Rendt, and G. Salama. Optical mapping of repolarization and refractoriness from intact hearts. *Circulation* 90:1469–1480, 1994.

[5] Girouard, S. D., K. R. Laurita, and D. S. Rosenbaum. Unique properties of cardiac action potentials recorded with voltage-sensitive dyes. *J. Cardiovasc. Electrophys.* 7:1024–1038, 1996.

[6] Girouard, S. D., J. M. Pastore, K. R. Laurita, K. W. Gregory, and D. S. Rosenbaum. Optical mapping in a new guinea pig model of ventricular tachycardia reveals mechanisms for multiple wavelengths in a single reentrant circuit. *Circulation* 93:603–613, 1996.

[7] Gray, R. A., J. Jalife, A. Panfilov, W. T. Baxter, C. Cabo, J. M. Davidenko, and A. M. Pertsov. Nonstationary vortexlike reentrant activity as a mechanism of polymorphic ventricular tachycardia in the isolated rabbit heart. *Circulation* 91:2454–2469, 1995.

[8] Gray, R. A., A. M. Pertsov, and J. Jalife. Incomplete reentry and epicardial breakthrough patterns during atrial fibrillation in the sheep heart. *Circulation* 94:2649–2661, 1996.

[9] Knapp, C. H., and G. C. Carter. The generalized correlation method for estimation of time delay. *IEEE Trans. Acoust., Speech, Signal Process.* 24:320–327, 1976.

[10] Knisley, S. B. Transmembrane voltage changes during unipolar stimulation of rabbit ventricle. *Circ. Res.* 77:1229–1239, 1995.

[11] Kuglin, C. D., and D. C. Hines. The phase correlation image alignment method. *Proceedings of the 1975 International Conference on Cybernetics and Society*. San Francisco, CA: IEEE, 1975, pp. 163–165.

[12] Loew, L. M. Potentiometric dyes: Imaging electrical activity of cell membranes. *Pure Appl. Chem.* 68:1405–1409, 1996.

[13] Ni, Q., R. S. MacLeod, R. L. Lux, and B. Taccardi. A novel interpolation method for electric potential fields in the heart during excitation. *Ann. Biomed. Eng.* 26:597–607, 1998.

[14] Pertsov, A. M., J. M. Davidenko, R. Salomonsz, W. T. Baxter, and J. Jalife. Spiral waves of excitation underlie reentrant activity in isolated cardiac muscle. *Circ. Res.* 72:631–650, 1993.

[15] Reiter, M. J., M. Landers, Z. Zetelaki, C. J. H. Kirchhof, and M. A. Allessie. Electrophysiological effects of acute dilation in the isolated rabbit heart: Cycle length-dependent effects on ventricular refractoriness and conduction velocity. *Circulation* 96:4050–4056, 1997.

[16] Rogers, J. M., and A. D. McCulloch. Nonuniform muscle fiber orientation causes spiral wave drift in a finite element model of cardiac action potential propagation. *J. Cardiovasc. Electrophysiol.* 5:496–509, 1994.

[17] Rohr, S., and B. M. Salzberg. Multiple site optical recording of transmembrane voltage (MSORTV) in patterned growth heart cell cultures: Assessing electrical behavior, with microsecond resolution, on a cellular and subcellular scale. *Biophys. J.* 67:1301–1315, 1994.

[18] Sung, D., J. H. Omens, and A. D. McCulloch. Model-based analysis of optically mapped epicardial activation patterns and conduction velocity. *Ann. Biomed. Eng.* 28:1085–1092, 2000.

[19] Windisch, H., H. Ahammer, P. Schaffer, W. Muller, and D. Platzer. Optical multisite monitoring of cell excitation phenomena in isolated cardiomyocytes. *Pflugers Arch.* 430:508–518, 1995.

[20] Witkowski, F. X., L. J. Leon, R. B. Clark, M. L. Spano, W. L. Ditto, and W. R. Giles. A method for visualization of ventricular fibrillation: Design of a cooled fiberoptically coupled image intensified CCD data acquisition system incorporating wavelet shrinkage based adaptive filtering. *Chaos* 8:94–102, 1998.